MATERIALS CHEMISTRY FRONTIERS

RESEARCH ARTICLE

View Article Online
View Journal | View Issue

Cite this: *Mater. Chem. Front.*, 2022, **6**, 2859

Cucurbit[6]uril-based carbon dots for recognizing L-tryptophan and capecitabine†

Ming Liu,[a] Ran Cen,[a] Ji-Hong Lu,[a] Tie-Hong Meng,*[b] Chun-Rong Li,[b] Carl Redshaw,*[c] Timothy J. Prior,[c] Zhu Tao[a] and Xin Xiao*[a]

Received 20th June 2022,
Accepted 17th August 2022

DOI: 10.1039/d2qm00589a

rsc.li/frontiers-materials

Fluorescent nitrogen and fluorine doped carbon dots (CDs) were prepared by a hydrothermal method using levofloxacin (LVFX) and cucurbit[6]uril (Q[6]) as the nitrogen and carbon sources, respectively. Decomposition of LVFX occurred at elevated temperature affording *N*,*N*′-desethylene levofloxacin hydrochloride (*N*,*N*′-DLH). The crystal structure of the resulting inclusion complex *N*,*N*′-DLH@Q[6]·$[CdCl_4]_2(H_3O)\cdot 9H_2O$ was determined, where *N*,*N*′-DLH is protonated on each of the terminal nitrogens and the quinone functionality is a quinol which forms an intramolecular hydrogen bond to the carboxylic acid. The synthesized *N*,*N*′-DLH containing Q[6]-CDs emitted intense blue fluorescence with high photostability and exhibited stability at high ionic strength. In particular, the original rigid macrocyclic skeletons of these hosts were retained during the fabrication process, which helps in uniquely distinguishing them from other reported CDs. Meanwhile, the performance of the Q[6]-CDs was characterized using fluorescence and NMR spectroscopies. Subsequently, using the obtained Q[6]-CDs, an efficient sensing method for L-tryptophan (L-Trp) and capecitabine (CAP) has been developed based on macrocyclic host–guest chemistry. Under applicable conditions, the detection limits for L-Trp and CAP were calculated to be 5.13×10^{-8} M and 1.48×10^{-8} M, respectively.

Introduction

Carbon dots (CDs) have attracted extensive attention in recent years because of their excellent optical and chemical properties and have many potential applications.[1,2] CDs were discovered by accident during the processing of single-walled carbon nanotubes (SWCNT).[3] Carbon dots (CDs), as one of the important family members of carbon-based materials, not only have similar physical and chemical properties to those of representative carbon-based materials, but also exhibit low toxicity, photostability, biocompatibility, multiphoton excitation, upconversion photoluminescence and chemiluminescence.[4,5] These excellent characteristics mean that CDs are widely used in the sensing and biomedical fields.[6–8] In addition, because of their good biocompatibility and photostability, CDs can be considered as an excellent substitute for more toxic semiconductor quantum dots or unstable organic fluorophores (for biological applications).[9–11] With the development of research on CDs, researchers have put forward a number of simple synthetic methods, such as laser ablation, pyrolysis, electrochemical synthesis, supported synthesis, acid oxidation, microwave-assisted synthesis and hydrothermal synthesis.[12–17] Among them, CDs synthesized by hydrothermal methods can generate hydroxyl groups, carbonyl groups, carboxyl groups, ether groups, epoxy groups, *etc.* at the surface. These groups usually have good reactivity, thus affording these nanoparticles excellent reactivity.[18] Therefore, the direct preparation of CDs with adjustable particle size and fluorescence characteristics in water has broad application prospects. Here, cucurbit[*n*]urils are also shown to be a good raw material for CD synthesis.

Cucurbit[*n*]urils[19,20] (usually abbreviated as Q[*n*]s or CB[*n*]s, *n* = 5–8, 10, 13–15) are macrocyclic compounds. Generally speaking, Q[*n*]s possess a rigid cavity and two open ports, with the latter composed of multiple carbonyl oxygens and they have excellent molecular selective binding ability in water. Therefore, cucurbit[*n*]urils play an important role in supramolecular chemistry and material science.[21–24] In Q[*n*]s, the nearly neutral charge distribution on the cavity surface is beneficial to the combination of guest molecules and the formation of host–guest inclusion compounds.[25–35] However, Q[*n*] homologues have some disadvantages, such as poor solubility of Q[*n*]s homologues in pure water, insolubility in most organic solvents, difficulty in functional

[a] *Key Laboratory of Macrocyclic and Supramolecular Chemistry of Guizhou Province, Institute of Applied Chemistry, Guizhou University, Guiyang, 550025, China. E-mail: gyhxxiaoxin@163.com, xxiao@gzu.edu.cn*
[b] *Public Course Teaching Department, Qiannan Medical College for Nationalities, Duyun, 558000, China. E-mail: mengtiehong19850@163.com*
[c] *Department of Chemistry, University of Hull, Hull, HU6 7RX, UK. E-mail: C.Redshaw@hull.ac.uk*

† Electronic supplementary information (ESI) available. CCDC 2161127. For ESI and crystallographic data in CIF or other electronic format see DOI: https://doi.org/10.1039/d2qm00589a

modification of Q[*n*]s homologues and no absorption in the visible region. However, research shows that the synthesis of CDs with Q[*n*]s as the source material has the unique advantage of producing CDs from a single organic precursor, that is, it has the advantages of high crystallinity, adjustable fluorescence emission, long fluorescence lifetime and high quantum yield through a simple solvent method. Therefore, we can further expand and improve the application and properties of Q[*n*]s by introducing CDs. As we know, carbon dots have excellent water solubility and are readily functionalized, which can make up for the deficiencies of the Q[*n*]s. Recently, our research group introduced Q[*n*]s into the preparation of carbon dots to synthesize a new type of carbon dot. The Q[6]-CDs, Q[7]-CDs and Q[8]-CDs were prepared by hydrothermal methods using Q[*n*]s (*n* = 6, 7, 8). These results showed that the rigid structure of the Q[*n*]s remains intact, and the obtained Q[*n*]-CDs (*n* = 6, 7, 8) exhibited good biocompatibility and fluorescence labeling during cytotoxicity and cell imaging experiments.[36,37] On the other hand, in order to improve the luminescent properties of CDs, the introduction of heteroatoms such as N, B, S, P, Si and Se in the hydrothermal synthesis of CDs has proved to be an effective strategy.[38–43] Fluorine is an element with high electronegativity, which can improve the fluorescence properties of CDs. F-doped CDs have the advantages of biocompatibility, cell absorption and stability.[44] However, up to now, there are few research reports on F-doped CDs.

In this paper, carbon dots based on Q[6] were synthesized by using Q[6] and levofloxacin (LVFX) containing C, N, O and F as potential carbon sources. For convenience of description, we refer to these as Q[6]-CDs herein. Q[6]-CDs with high solubility and stability were synthesized by hydrothermal synthesis. The Q[6]-CDs were obtained by simply controlling the fusion and carbonization of LVFX with the aromatic skeleton structure substituted by C, N, O and F with Q[6] in water. Scheme 1 depicts the structural diagram of Q[6] and LVFX.

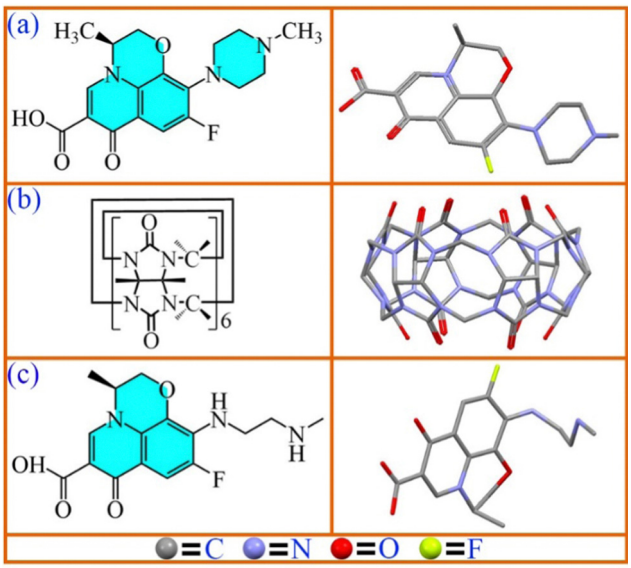

Scheme 1 Structures of (a) LVFX; (b) Q[6]; (c) *N*,*N*′-DLH.

However, it is worth mentioning that research has shown that LVFX can be oxidized and degraded at high temperature, or by light and other factors during either preparation or storage, and *N*,*N*′-desethylene levofloxacin hydrochloride (*N*,*N*′-DLH) is one of the important impurities.[45] In this work, the carbon dots synthesized by LVFX and Q[6] were prepared at 180 °C. Given this, the LVFX present decomposes into *N*,*N*′-DLH, and the obtained carbon dots result from the combination of *N*,*N*′-DLH and Q[6]. Furthermore, the single crystal structure of LVFX and Q[6], prepared from a sample synthesized at high temperature, also revealed that the guest molecule LVFX had decomposed. Significantly, it is found that the carbon dots assembled from Q[6] and *N*,*N*′-DLH possessed excellent fluorescence properties. These results provide insight into the degradation properties of LVFX, as well as a strategy for forming carbon dots incorporating *N*,*N*′-DLH. Thanks to the advantages of Q[6]-CDs, such as good water solubility, excellent fluorescence, high sensitivity and fast response, the Q[6]-CDs were selected as the fluorescent probe, and 20 essential amino acids and the anti-tumor drug capecitabine (CAP) agent were identified and detected. It was found that the Q[6]-CDs were specific and sensitive for the detection of L-tryptophan (L-Trp) and capecitabine (CAP). At the same time, we also preliminarily studied the possible interaction mechanism of the functionalized Q[6]-CDs with L-Trp and CAP, respectively. On this basis, the application of Q[6]-CDs in the fluorescence detection and identification of L-Trp and CAP is further broadened. This work also lays down the foundation for the detection of L-Trp and CAP in cells, and provides a new application for such CDs.

Experimental

Chemicals and reagents

Q[6] was synthesized according to the literature.[46] Levofloxacin, capecitabine and all amino acids were purchased from Aladdin (Shanghai, China). Deionized water was used throughout. All amino acids and capecitabine were prepared with deionized water in a solution of 0.02 M concentration.

Apparatus and Instruments

^{1}H NMR spectral experiments were carried out on a Nippon Denshi JEOL FT-400 spectrometer. The UV-vis spectra were recorded at room temperature using an 8453 UV-vis spectrophotometer purchased from Agilent (Agilent Technologies, Santa Clara, California, USA). Fluorescence spectra measurements were performed on a Varian Cary Eclipse fluorescence spectrophotometer equipped with a xenon discharge lamp. A model 818 pH meter (Orilon of America) was used to adjust the pH of the solution. Fourier transform infrared (FTIR) spectra were recorded on a Bruker Vertex as KBr pellets. Crystallographic data were collected on a Bruker D8 VENTURE diffractometer using graphite monochromated Mo Kα radiation (λ = 0.71073 Å).

^{1}H NMR measurements

^{1}H NMR spectra were recorded on a JEOL JMM-ECZ400s spectrometer at 25 °C. D_2O was used as a field frequency lock,

and the observed chemical shift is reported in parts per million (ppm) relative to the built-in tetramethylsilane (TMS) standard (0.0 ppm).

Fourier transform infrared spectroscopy (FTIR) sample

The above Q[6]-CDs and spectrally pure potassium bromide were dried in a vacuum drying oven and mixed at a ratio of about 1 : 200. The mixture was thoroughly ground and mixed in an agate mortar, and then the tablets were pressed on a pressure machine for sample preparation using the matching mold of an infrared spectrometer. The absorption/transmission spectrum was recorded by an infrared spectrometer with a scanning range of 400–4000 cm^{-1}.

Preparation of UV-vis solution

10 mg Q[6]-CDs solid was dissolved in 25 mL ultrapure water to obtain a concentration of 400 μg mL^{-1} reserve solution. Then 5 mL of the reserve solution was diluted to 100 mL with ultrapure water to obtain 20 μg mL^{-1} Q[6]-CDs solution. 3 mL of the 20 μg mL^{-1} solution was transferred into a UV cuvette, and the UV-visible absorption spectrum of the Q[6]-CDs was measured by UV-visible spectrophotometer (scanning speed was medium, scanning range was 200–800 nm).

Preparation of fluorescence spectrum (FL) solution

3 mL of 20 μg mL^{-1} solution was transferred into a fluorescence colorimetric dish, and the fluorescence emission spectrum of the Q[6]-CDs was measured by fluorescence spectrophotometer. The fluorescence emission spectra of the carbon quantum dot solution in each centrifuge tube excited at 245 nm were measured.

Detection of amino acids by Q[6]-CDs

Different amino acids (L-Ser, L-Aal, L-Phe, L-Asn, L-Leu, L-Thr, L-Pro, L-Lys, L-Arg, L-Tyr, L-Cys, L-Gly, L-Ala, L-Iso, L-Gln, L-Asp, L-Met, L-Glu, L-His, L-Trp) were added into the prepared fluorescent probe standard solution (3 mL, 20 μg mL^{-1}) for detection (the added amino acid concentration is 0.02 mol L^{-1}, and the volume is 50 μL). The fluorescence emission spectra of the carbon quantum dot solution in each centrifuge tube excited at 245 nm were measured, and the change of fluorescence intensity was compared with that of blank solution without the amino acids.

Detection of capecitabine by Q[6]-CDs

CAP was added into the prepared fluorescent probe standard solution (3 mL, 20 μg mL^{-1}) for detection (the added CAP concentration is 0.02 mol L^{-1}, and the volume is 50 μL). The fluorescence emission spectra of the carbon quantum dot solution in each centrifuge tube excited at 245 nm were measured, and the change of fluorescence intensity was compared with that of blank solution without CAP.

Synthesis and purification of Q[6]-CDs

LVFX (20 mg, 0.05 mM) and Q[6] (50 mg, 0.05 mM) were dissolved in deionized water (50 mL). The solution was stirred for 60 min and the solution was transferred into a Teflon autoclave. After being heated at 180 °C for 12 h, the autoclave was cooled to room temperature. The reaction solution was centrifuged at 4000 rpm for 45 min, and the supernatant was collected. The resulting supernatant was further filtered through a 0.22 mm filter membrane to remove the large or agglomerated particles. After removing the solvents and freeze-drying, a brown powder was obtained (35 mg, yield 50%).

Results and discussion

Characterization of Q[6]-CDs

The Q[6]-CDs were synthesized from pure LVFX and Q[6] using a conventional hydrothermal route (for details, see the Experimental section). In the UV/vis spectra, the Q[6]-CDs exhibited maximum adsorption peaks at 275 nm in an aqueous solution (Fig. 1a). The absorption peak at 275 nm was attributed to the $\pi \rightarrow \pi^*$ transitions of the C=C bonds. Interestingly, the solution of Q[6]-CDs emitted a blue fluorescence (λ_{max} = 430 nm) (Fig. 1b). No UV-vis adsorption and emission behaviour was observed in the aqueous solutions of pristine Q[6].

In order to better understand the role of Q[6] in the formation of Q[6]-CDs, the host–guest interaction between LVFX and Q[6] was studied before the hydrothermal reaction. First, a pH titration of LVFX and the LVFX@Q[6] complex over the range pH 2–12.0 was performed using UV/vis spectra, as shown in Fig. S1 (ESI†). For the free LVFX and LVFX@Q[6], minimal changes in the UV-vis absorption spectra were observed at pH $\leq$ 5 and pH $\geq$ 7, but there was a significant change in the absorption spectra at λ = 288 nm between pH 5.0 and 7.0. To study the binding interaction of LVFX with Q[6], subsequent investigations were carried out on a solution of pH 7.0. Subsequently, according to the ^{1}H NMR spectra of Q[6] and LVFX, the interaction between Q[6] and LVFX was studied. As shown in Fig. S2, (ESI†) after the addition of 1.0 equiv. of Q[6], H_i, H_j, H_a, H_b, H_c, H_d, H_e, H_g and H_f the proton peaks corresponding to LVFX were shifted downfield, and the groups of the LVFX guest are located at the portals of the host. Meanwhile, the ^{1}H NMR spectra of *N*,*N*′-DLH@Q[6], LVFX@Q[6] and Q[6]-CDs were compared (Fig. S3, ESI†). It is evident that the Q[6]-CDs contain *N*,*N*′-DLH, which is the result of the oxidative decomposition of LVFX following exposure to high temperature. We then carried out a series of studies on these Q[6]-CDs.

At the same time, the fluorescence spectrum of free LVFX indicated that the organic precursor exhibited a greenish blue emission with the maximum wavelength at around 470 nm at room temperature in water, and the UV-vis absorption and fluorescence emission changes were observed upon the addition of the Q[6] host to the LVFX solution with a 1 : 1 binding fashion (host/guest, mole ratio) (Fig. S4, ESI†), which further supported the portal binding model of the Q[*n*]s. Importantly, the original proton peaks of Q[6] were observed in the ^{1}H NMR spectrum of the Q[6]-CDs (Fig. S5, ESI†), which indicated that the rigid macrocyclic skeleton of the Q[6] remained intact during the hydrothermal reaction with LVFX.

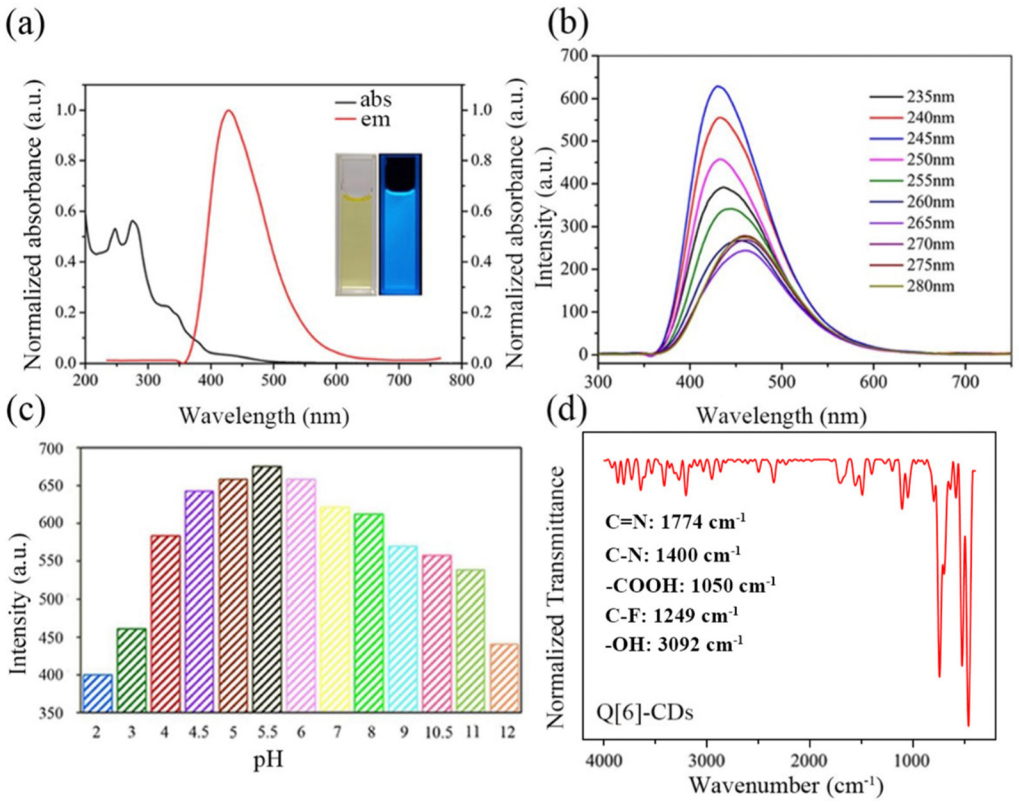

Fig. 1 (a) UV-vis absorption, fluorescence excitation and emission spectra of the Q[6]-CDs. Inset: Photographs of the solution of the Q[6]-CDs under daylight (left) and 365 nm UV light (right); (b) the emission spectra of the Q[6]-CDs under different excitation wavelengths ranging from 235 to 280 nm; (c) fluorescence responses of the Q[6]-CDs in different pH solutions; (d) FI-IR spectra.

Then, we studied the effect of pH on the fluorescence properties of the Q[6]-CDs (Fig. 1c). Research has found that the fluorescent emission intensity of the Q[6]-CDs rises to the largest value at pH 5.5, with the solution pH changing from 2 to 5.5, and then decreases as the pH changes from 5.5 to 12.0. This shows that the Q[6]-CDs are very sensitive to pH. Such behaviour is similar to CDs containing hydroxyl and carboxyl moieties.[47]

In addition, to better understand the difference between the groups LVFX@Q[6] and Q[6]-CDs, the FT-IR spectra were analyzed to identify surface functional groups of LVFX@Q[6] (Fig. S6 and Table S1, ESI†). The strong absorption peaks at 1774 and 1734 cm^{-1} are assigned to the stretching vibrations of C═N and C═O, respectively.[48,49] The sharp peaks at 1684 cm^{-1} and 1490 cm^{-1} are in accord with the C═O stretching and N–H bending.[50] However, the FT-IR spectrum also confirmed that the Q[6]-CDs contains functional groups of −OH (3092 cm^{-1}) and C═O (1705 cm^{-1}),[51] and –C–N (1400 cm^{-1}), –C–O and –C–O–C (1000–1200 cm^{-1}),[52] –COOH (1050 cm^{-1}) were present. New absorption bands belonging to the stretching vibration of –C–H (2867 cm^{-1}, 2951 cm^{-1}) in the Q[6]-CDs,[53] and the stretching vibrations of C–F bond at 1249 cm^{-1} were observed[54] (Fig. 1d). Furthermore, the structure and morphology of the Q[6]-CDs were characterized by transmission electron microscope (Fig. S7, ESI†) and X-ray powder diffraction (Fig. S8, ESI†).

Also, the chemical composition of the Q[6]-CDs was determined by X-ray photoelectron spectroscopy. Fig. 2a shows clear peaks for C1s, N1s, O1s and F1s, and the samples were located at 286.18, 400.38, 532.38 and 687.38 eV, respectively, indicating that the samples were mainly composed of C, O, N and F elements. The elemental contents of the Q[6]-CDs was found to be C, 67.29%, N, 14.65%, O, 16.13%, F, 1.94%, respectively. The higher C and O content confirmed that the Q[6]-CDs are rich in oxygen-containing functional groups. Fig. 2b shows the fine spectrum of C1s, and the absorptions at 286.18 eV, and 289.18 eV, which indicate the existence of C–C/C═C, and C═O bonds, respectively. In the N1s spectra (Fig. S9, ESI†), absorptions at 400.38 eV can be attributed to C–N bonds. In the case of the O1s spectra (Fig. 2c), absorptions at 532.38 eV correspond to C═O and C–OH bonds. In the F1s spectra (Fig. 2d), absorptions at 687.38 eV can be attributed to C–F bonds. The presence of the C═C, C–N, C═O, C–OH, and C–F bonds further verified that Q[6]-CDs were successfully synthesized. The presence of these hydrophilic functional groups enhances the water solubility and stability of the Q[6]-CDs, thereby making the *m*-Q[6]-CQDs highly dispersed and stable in aqueous solution. At room temperature, the fluorescence decay time of Q[6]-CDs were tested (excited by a 375 nm LD pump), see Fig. S10 (ESI†). Using a single exponential fitting, the fluorescence lifetime of Q[6]-CDs was fitted at 10.84 ns, and the quantum yield of Q[6]-CDs is 0.51% (Fig. S11, ESI†).

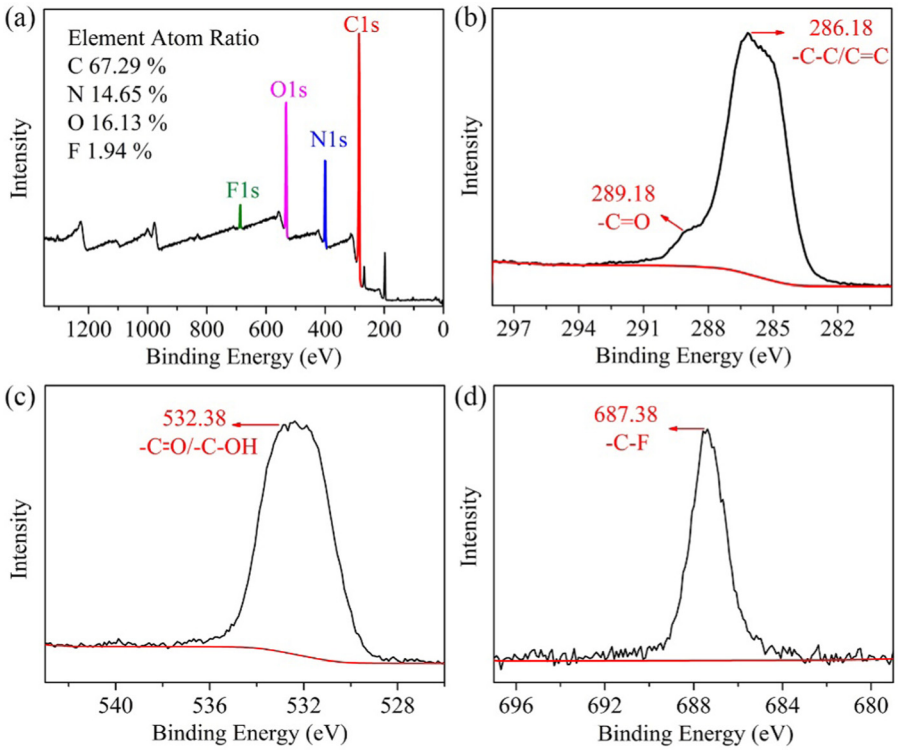

Fig. 2 (a) XPS spectra of the Q[6]-CDs; (b–d) high resolution spectra of C1s, O1s and F1s, respectively.

Description of the crystal structure of *N*,*N*′-DLH@Q[6]

The X-ray crystal structure analysis provided unequivocal proof of the 1 : 1 binary complex assembly (Fig. 3). The crystal structure reveals that hydrogen bonding is the dominant interaction driving the formation of *N*,*N*′-DLH@Q[6]·$[CdCl_4]_2(H_3O)\cdot 9H_2O$ (Fig. 3). Table S2 (ESI†) provides the crystal data and structure refinement for *N*,*N*′-DLH@Q[6]·$[CdCl_4]_2(H_3O)\cdot 9H_2O$. Meanwhile, as shown in Fig. S12, (ESI†) the ^{1}H NMR spectrum of the *N*,*N*′-DLH@Q[6]·$[CdCl_4]_2(H_3O)\cdot 9H_2O$ sample was analyzed.

The host–guest complex *N*,*N*′-DLH@Q[6]·$[CdCl_4]_2(H_3O)\cdot 9H_2O$ was prepared from Q[6] and the *N*,*N*′-DLH using host–guest chemistry to direct the non-covalent interactions. Single-crystal X-ray diffraction revealed that there are two different intermolecular forces in the unit cell of *N*,*N*′-DLH@Q[6]·$[CdCl_4]_2(H_3O)\cdot 9H_2O$, as shown in Fig. 3. The protonation of the guest helps to facilitate two hydrogen bonds between N25 and the Q6 as shown below. Note the *N*,*N*′-DLH is thrice protonated at the each of the terminal nitrogens and the quinone functionality is a quinol; the latter forms an intramolecular hydrogen bond to the carboxylic acid. Interestingly, the guest has racemised during the synthesis, *i.e.* it is no longer racemically pure at the ethylene bridge attached to the ring system.

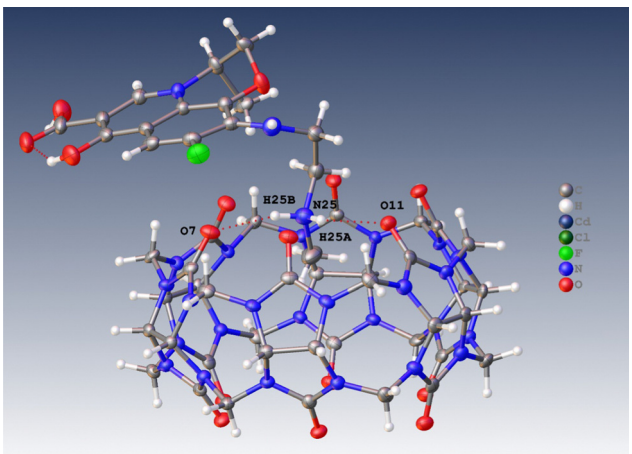

Fig. 3 The host–guest interactions. Hydrogen bonds are shown as dashed lines. Minor disorder is not shown.

There is minor disorder in the positions of the unbound water molecules and some are split over two positions. It was not possible to locate hydrogen atoms on these. Similarly, it was not possible to identify the location of the single H_3O^+ ion. There is good evidence for the protonation of the guest molecule. Electron density consistent with the presence of hydrogen atoms is found on the atoms N25, N26, and O13 suggesting that these atoms are protonated. Similarly, the bond C41–N26 is too short to be a single bond and the bond C46–O13 is too long to be a double bond; the hydrogen attached to O13 also forms an intramolecular hydrogen bond to O14. For a view of the asymmetric unit and the guest see Fig S13 and S14 (ESI†).

Fluorescence detection of the Q[6]-CDs towards L-tryptophan

For practical detection, a favorable fluorescent probe should have high selectivity to the analyte. Herein, the fluorescence response of Q[6]-CDs to a series of common amino acids was

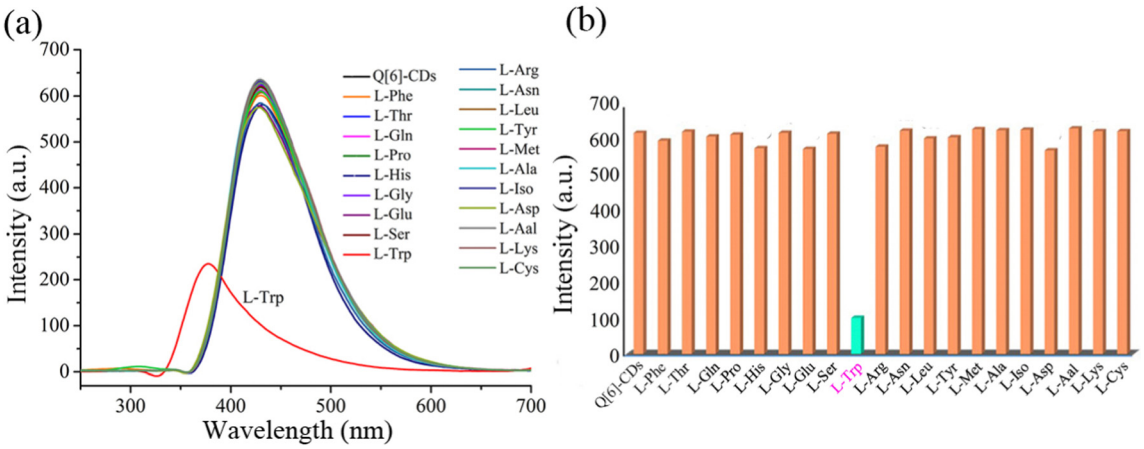

Fig. 4 Fluorescence response of Q[6]-CDs (20 μg mL^{-1}; λ_{max} = 430 nm) to amino acids (amino acids (aq.), 10 μM.): (a) emission spectra of each amino acid (aq.); (b) bar chart showing the intensities obtained from the addition of each amino acid (aq).

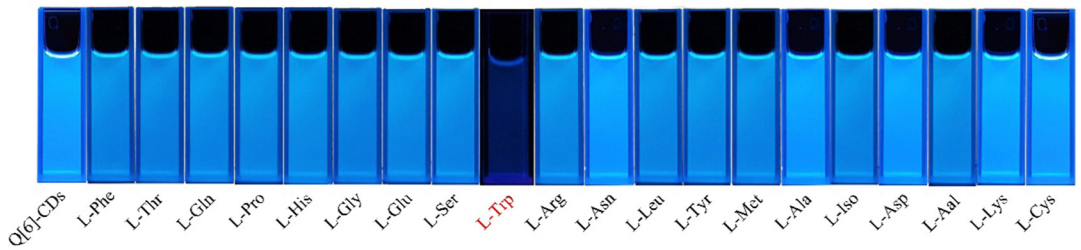

Fig. 5 Photographic images of the Q[6]-CDs solutions containing various amino acids under UV light (365 nm).

determined. When L-Trp was added to an aqueous solution of Q[6]-CDs, the fluorescence intensity at 430 nm was strongly reduced (Fig. 4), and was accompanied by an obvious blue shift of 52 nm, while the addition of the other 19 amino acids did not cause any significant fluorescence changes for the Q[6]-CDs. This demonstrated the potential of the prepared Q[6]-CDs for the detection of L-Trp, and except for L-Trp, the remaining 19 amino acids had no significant effect on the fluorescence intensity at 430 nm (Fig. 5).

To further understand the recognition capability of the Q[6]-CDs toward L-Trp, luminescence titration experiments were performed. Fig. 6a shows that the fluorescence intensity of the Q[6]-CDs decreases gradually, and the fluorescence emission of the Q[6]-CDs was tunable from 430 to 378 nm with the continuous addition of L-Trp. The increasing intensity was accompanied by a clearly enhanced UV-vis absorption intensity upon the addition of an increasing concentration of L-Trp to an aqueous solution of the Q[6]-CDs (Fig. S15, ESI†). In addition, the fluorescence intensity observed at 430 nm exhibited a good linear relationship with the L-Trp concentration over the range of 0.75–1.8 μM (Fig. 6b), and the LOD was calculated to be 5.13×10^{-8} M. This indicated that the Q[6]-CDs were very sensitive toward the detection of L-Trp in aqueous media. To evaluate the selectivity of the Q[6]-CDs towards L-Trp detection, the effects of the co-existing amino acids were investigated under the same conditions. As shown in Fig. S16, (ESI†) the other amino acids showed insignificant interference on the determination of L-Trp within the linearity range.

The detection mechanism of the Q[6]-CDs probe towards L-Trp was analyzed by ^{1}H NMR spectroscopy. As shown in Fig. S17, (ESI†) the ^{1}H NMR spectra of the interactions of L-Trp with Q[6] clearly indicates that the peaks corresponding to H_a–H_e on the indole moiety of the Trp gradually shifted upfield ($\Delta\delta$:H_a and H_e, 0.04 ppm; H_c and H_d, 0.03 ppm; H_b, 0.05 ppm). Conversely, it became apparent that the proton H_g of Trp was shifted downfield ($\Delta\delta$: H_f, 0.03 ppm; H_g, 0.07 ppm). This study implied that the indole moiety of Trp can be encapsulated by the cavity of Q[6]. In addition, the spectra are shown in Fig. S18 (ESI†). In the presence of the Q[6]-CDs, all proton signals of the L-Trp underwent an obvious shift upfield. For example, the signals of protons H_b, H_d, H_c,H_a, H_e, H_g, and H_f on the L-Trp significantly shifted upfield ($\Delta\delta$ = 0.09, 0.09, 0.18, 0.09, 0.08, 0.05 and 0.08 ppm, respectively).

Similar NMR spectral changes were observed in the LVFX and L-Trp systems. As the concentration of LVFX was increased to ~1.0 eq., for the L-Trp guests, the signals of all the guest protons move upfield by different degrees (Fig. S19, ESI†). Therefore, the results show that the possible mechanism of Q[6]-CDs fluorescence quenching caused by the addition of L-Trp is that the indole part of L-Trp is a planar aromatic ring structure. At the same time, the main chromophores (conjugated π domain and molecular fluorophore) in the Q[6]-CDs are

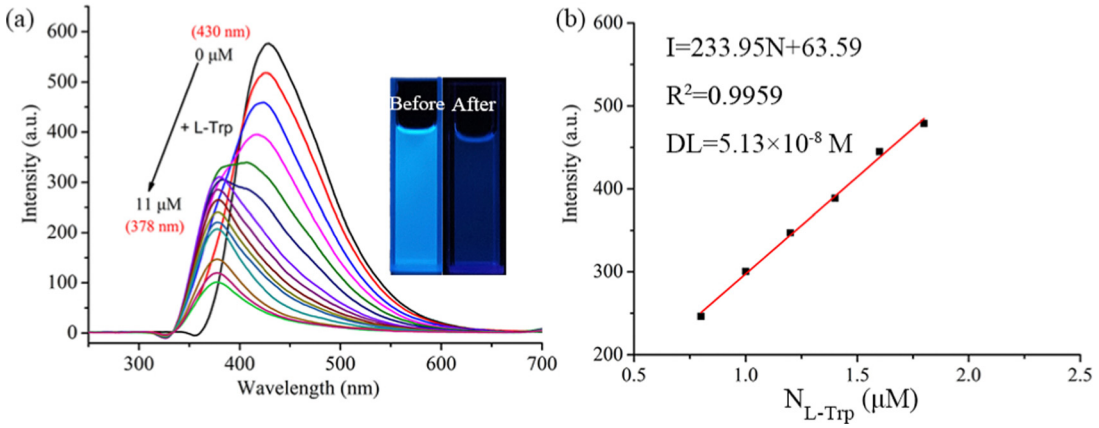

Fig. 6 Titration fluorescence spectra of Q[6]-CDs (20 μg mL^{-1}) with L-Trp (0, 0.2, 0.3,...11.0 μM). (a) Emission spectra; (b) the DL of the Q[6]-CDs for L-Trp.

also planar aromatic ring structures. Due to their strong intermolecular π–π stacking interaction, their large planar polycyclic aromatic structure promotes them to stack in a directional way, which will lead to the nonradiative transition of the excited state back to the ground state, resulting in fluorescence quenching.[55]

Analytical performance of Q[6]-CDs towards capecitabine

Capecitabine can prolong the survival time of various cancer patients, and is widely used in the treatment of advanced primary or metastatic breast cancer, rectal cancer, colon cancer and gastric cancer. Therefore, it is very important to choose a sensor to identify and detect CAP. With this in mind, we have probed the ability of the Q[6]-CDs to detect CAP. As shown in Fig. 7, when CAP is added to the Q[6]-CDs solution, the fluorescence intensity is quenched at 430 nm, and the emission wavelength is blue shifted from 430 nm to 396 nm. Furthermore, with the gradual dropping of CAP into the Q[6]-CDs solution, the UV-vis absorption intensity of the system gradually increases (Fig. S20, ESI†). The mechanism of the fluorescence quenching caused by the addition of CAP to Q[6]-CDs was next investigated. Firstly, the ^{1}H NMR spectrum (Fig. S21, ESI†) of the CAP titration Q[6] was analyzed. It can be seen from the figure that when the molar ratio of CAP to Q[6] is 1 : 1, only the alkyl chain (H_a, H_b, H_c, H_d) in the CAP molecule shifts upfield, and the rest shift downfield, which indicates that only the alkyl chain of the CAP extends into the cavity of the Q[6]. In addition, the interaction between CAP and Q[6]-CDs was further analyzed by ^{1}H NMR spectroscopy (Fig. S22, ESI†), and it was found that all protons of the CAP molecule shift upfield. In order to explain this phenomenon, the NMR spectrum of the interaction between CAP and LVFX was analyzed (Fig. S23, ESI†). It was found that when the same amount of CAP was dripped into LVFX, all the protons of the CAP molecules also shifted upfield. Therefore, the reason of fluorescence quenching caused by the addition of CAP to Q[6]-CDs is similar to the above-mentioned L-Trp system, and it may also be due to the planar aromatic ring structure of the CAP. There is π–π stacking between the planar aromatic ring structure of CAP and the planar aromatic ring structure in Q[6]-CDs, and the polycyclic aromatic structure between them forces them to stack in a directional way. This accumulation will cause the excited state to transition back to the ground state by nonradiative pathway, resulting in fluorescence quenching.

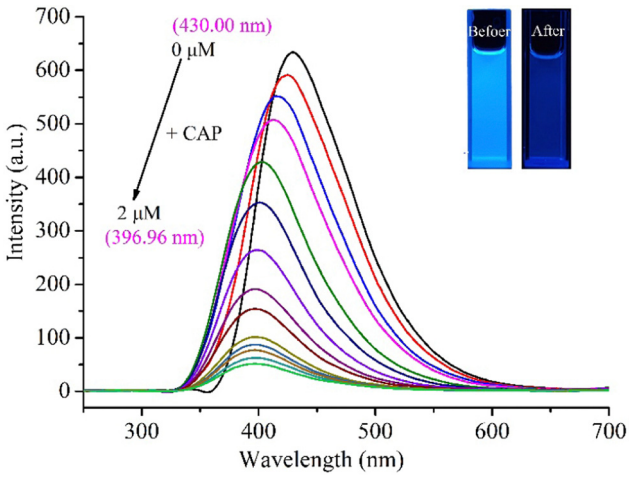

Fig. 7 Titration fluorescence spectra of Q[6]-CDs (20 μg mL^{-1}) with CAP (0, 0.05, 0.1,...2.0 μM.).

Conclusions

In this paper, Q[6] and LVFX were used as carbon sources, and Q[6]-CDs were synthesized by simply controlling the fusion and carbonization of LVFX with Q[6]. At the same time, it was found that there is *N*,*N*′-DLH in the Q[6]-CDs, which is due to the high temperature degradation of LVFX to *N*,*N*′-DLH, whereby the piperazine ring of LVFX has decomposed into an ethylenediamine group. The Q[6]-CDs have the advantage of high sensitivity, fast response, good selectivity, high water solubility and excellent fluorescence performance. The Q[6]-CDs, as a new water-soluble nano-sensor, can efficiently and simply detect L-Trp and CAP. The detection limits of Q[6]-CDs for L-Trp and

CAP are 5.13×10^{-8} M and 1.48×10^{-8} M, respectively. In addition, the possible mechanism of detecting L-Trp and CAP by Q[6]-CDs was analyzed, which may be due to the fact that both L-Trp and CAP have planar aromatic ring structures, and there is also a planar aromatic ring structure in the Q[6]-CDs. There is π–π stacking between the planar aromatic ring structures of L-Trp and CAP and the planar aromatic ring structures in Q[6]-CDs, respectively, and their large planar polycyclic aromatic structures force them to stack in a directional manner. This kind of accumulation will cause the excited state to transition back to the ground state by a non-radiative pathway, thus causing fluorescence quenching. This new type of fluorescence sensor has feasibility and potential application prospects in future fluorescence detection and identification.

Conflicts of interest

The authors declare no competing financial interest.

Acknowledgements

We thank the Science and Technology Fund of Guizhou Province ([2020]1Y051, ZK[2022]General552) and the Innovation Program for High-level Talents of Guizhou Province (No. 2016-5657) for financial support. CR thanks the EPSRC for an Overseas Travel Grant (EP/R023816/1).

References

1 J. Zhou, H. Zhou, J. B. Tang, S. Deng, F. Yan, W. J. Li and M. H. Qu, Carbon dots doped with heteroatoms for fluorescent bioimaging: a review, *Microchim. Acta*, 2017, **184**, 343–368.

2 (*a*) Y. Li, Y. Zhao, H. H. Cheng, Y. Hu, G. Q. Shi, L. M. Dai and L. T. Qu, Nitrogen-Doped Graphene Quantum Dots with Oxygen-Rich Functional Groups, *J. Am. Chem. Soc.*, 2012, **134**, 15–18; (*b*) M. Li, W. B. Wu, W. C. Ren, H. M. Cheng, N. J. Tang, W. Zhong and Y. W. Du, Synthesis and upconversion luminescence of N-doped graphene quantum dots, *Appl. Phys. Lett.*, 2012, **101**, 103107; (*c*) V. Talbo, J. Saint-Martin, S. Retailleau and P. Dollfus, Non-linear effects and thermoelectric efficiency of quantum dot-based single-electron transistors, *Sci. Rep.*, 2017, **7**, 1–13; (*d*) M. Ö. Alaş, A. Güngör, R. Genç and E. Erdem, Feeling the power: robust supercapacitors from nanostructured conductive polymers fostered with Mn^{2+} and carbon dots, *Nanoscale*, 2019, **11**, 12804–12816.

3 X. Xu, R. Ray, Y. Gu, H. J. Ploehn, L. Gearheart, K. Raker and W. A. Scrivens, Electrophoretic analysis and purification of fluorescent single-walled carbon nanotube fragments, *J. Am. Chem. Soc.*, 2004, **126**, 12736–12737.

4 Y. Han, D. Tang, Y. Yang, C. Li, W. Kong, H. Huang, Y. Liu and Z. Kang, Non-metal single/dual doped carbon quantum dots: a general flame synthetic method and electro-catalytic properties, *Nanoscale*, 2015, **7**, 5955–5962.

5 C. Hu, M. Li, J. Qiu and Y. P. Sun, Design and fabrication of carbon dots for energy conversion and storage, *Chem. Soc. Rev.*, 2019, **48**, 2315–2337.

6 J. Gu, X. Li, Z. Zhou, W. Liu, K. Li, J. Gao, Y. Zhao and Q. Wang, 2D MnO_2 nanosheets generated signal transduction with 0D carbon quantum dots: synthesis strategy, dual-mode behavior and glucose detection, *Nanoscale*, 2019, **11**, 13058–13068.

7 Y. Zhu, X. Ji, C. Pan, Q. Sun, W. Song, L. Fang, Q. Chen and C. E. Banks, A carbon quantum dot decorated RuO_2 network: outstanding supercapacitances under ultrafast charge and discharge, *Energy Environ. Sci.*, 2013, **6**, 3665–3675.

8 R. Wang, X. Wang and Y. Sun, One-step synthesis of self-doped carbon dots with highly photoluminescence as multifunctional biosensors for detection of iron ions and Ph, *Sens. Actuators, B*, 2017, **241**, 73–79.

9 Q. Li, T. Y. Ohulchanskyy, R. Liu, K. Koynov, D. Wu, A. Best, R. Kumar, A. Bonoiu and P. N. Prasad, Photoluminescent carbon dots as biocompatible nanoprobes for targeting cancer cells, *J. Phys. Chem. C*, 2010, **114**, 12062–12068.

10 Y. Wang, P. Anilkumar, L. Cao, J.-H. Liu, P. G. Luo, K. N. Tackett, S. Sahu, P. Wang, X. Wang and Y.-P. Sun, Carbon dots of different composition and surface functionalization: cytotoxicity issues relevant to fluorescence cell imaging, *Exp. Biol. Med.*, 2011, **236**, 1231–1238.

11 S. T. Yang, X. Wang, H. Wang, F. Lu, P. G. Luo, L. Cao, M. J. Meziani, J. H. Liu, Y. Liu, M. Chen, Y. Huang and Y. P. Sun, Carbon dots as nontoxic and high-performance fluorescence imaging agents, *J. Phys. Chem. C*, 2009, **113**, 18110–18114.

12 Y. Dong, R. Wang, H. Li, J. Shao, Y. Chi, X. Lin and G. Chen, Polyamine-functionalized carbon quantum dots for chemical sensing, *Carbon*, 2012, **50**, 2810–2815.

13 H. Ming, Z. Ma, Y. Liu, K. Pan, H. Yu, F. Wang and Z. Kang, Large scale electrochemical synthesis of high quality carbon nanodots and their photocatalytic property, *Dalton Trans.*, 2012, **41**, 9526–9531.

14 J. Zong, Y. Zhu, X. Yang, J. Shen and C. Li, Synthesis of photoluminescent carbogenic dots using mesoporous silica spheres as nanoreactors, *Chem. Commun.*, 2011, **47**, 764–766.

15 Z. Li, Y. Ni and S. Kokot, A new fluorescent nitrogen-doped carbon dot system modified by the fluorophore-labeled ssDNA for the analysis of 6-mercaptopurine and Hg(II), *Biosens. Bioelectron.*, 2015, **74**, 91–97.

16 J. Wang, S. Sahu, S. K. Sonkar, K. N. Tackett II, K. W. Sun, Y. Liu, H. Maimaiti, P. Anilkumar and Y. P. Sun, Versatility with carbon dots – from overcooked BBQ to brightly fluorescent agents and photocatalysts, *RSC Adv.*, 2013, **3**, 15604–15607.

17 Q. Liang, W. Ma, Y. Shi, Z. Li and X. Yang, Easy synthesis of highly fluorescent carbon quantum dots from gelatin and their luminescent properties and applications, *Carbon*, 2013, **60**, 421–428.

18 P. Roy, P. C. Chen, A. P. Periasamy, Y. N. Chen and H. T. Chang, Photoluminescent carbon nanodots: synthesis, physicochemical properties and analytical applications, *Mater. Today*, 2015, **18**, 447–458.

19 R. H. Gao, L. X. Chen, K. Chen, Z. Tao and X. Xiao, Development of hydroxylated cucurbit[*n*]urils, their derivatives and potential applications, *Coord. Chem. Rev.*, 2017, **348**, 1–24.
20 D. Yang, M. Liu, X. Xiao, Z. Tao and C. Redshaw, Polymeric self-assembled cucurbit[*n*]urils: Synthesis, structures and applications, *Coord. Chem. Rev.*, 2021, **434**, 213733.
21 M. Liu, Y. Zhou, L. X. Chen, B. Bian, X. Xiao and Z. Tao, Cucurbit[*n*]uril-calix[*n*]arene-based supramolecular frameworks assembled using the outer surface interactions of cucurbit[*n*]urils, *Chin. Chem. Lett.*, 2021, **32**, 375–379.
22 P. H. Shan, R. L. Lin, M. Liu, Z. Tao, X. Xiao and J. X. Liu, Recognition of Glycine by Cucurbit[5]uril and Cucurbit[6]-uril: A Comparative Study of Exo- and Endo-Binding, *Chin. Chem. Lett.*, 2021, **32**, 2301–2304.
23 J. Kim, I. S. Jung, S. Y. Kim, E. Lee, J. K. Kang, S. Sakamoto, K. Yamaguchi and K. Kim, New cucurbituril homologues: syntheses, isolation, characterization, and X-ray crystal structures of cucurbit[*n*]uril (*n* = 5, 7, and 8), *J. Am. Chem. Soc.*, 2000, **122**, 540–541.
24 A. I. Day, R. J. Blanch, A. P. Arnold, S. Lorenzo, G. R. Lewis and I. A. Dance, A cucurbituril-based gyroscane: a new supramolecular form, *Angew. Chem., Int. Ed.*, 2002, **41**, 285–287.
25 J. Lagona, P. Mukhopadhyay, S. Chakrabarti and L. Isaacs, The cucurbit[*n*]uril family., *Angew. Chem., Int. Ed.*, 2005, **44**, 4844–4870.
26 K. Kim, N. Selvapalam, Y. H. Ko, K. M. Park, D. Kim and J. Kim, Functionalized cucurbiturils and their applications, *Chem. Soc. Rev.*, 2007, **36**, 267–279.
27 R. N. Dsouza, U. Pischel and W. M. Nau, Fluorescent dyes and their supramolecular host/guest complexes with macrocycles in aqueous solution, *Chem. Rev.*, 2011, **111**, 7941–7980.
28 M. Liu, L. X. Chen, P. H. Shan, C. J. Lian, Z. H. Zhang, Y. Q. Zhang, Z. Tao and X. Xiao, Pyridine Detection Using Supramolecular Organic Frameworks Incorporating Cucurbit[10]uril, *ACS Appl. Mater. Interfaces*, 2021, **13**, 7434–7442.
29 W. Zhang, Y. Luo, J. Zhao, C. Zhang, X.-L. Ni, Z. Tao and X. Xiao, Controllable fabrication of a supramolecular polymer incorporating twisted cucurbit[14]uril and cucurbit[8]uril *via* self-sorting, *Chin. Chem. Lett.*, 2022, **33**, 2455–2458.
30 L. Isaacs, Stimuli responsive systems constructed using cucurbit[*n*]uril-Type molecular containers, *Acc. Chem. Res.*, 2014, **47**, 2052–2062.
31 K. I. Assaf and W. M. Nau, Cucurbiturils: from synthesis to high-affinity binding and catalysis, *Chem. Soc. Rev.*, 2015, **44**, 394–418.
32 Y. Luo, W. Zhang, M. Liu, J. Zhao, Y. Fan, B. Bian, Z. Tao and X. Xiao, A supramolecular fluorescent probe based on cucurbit[10]uril for sensing the pesticide dodine, *Chin. Chem. Lett.*, 2021, **32**, 367–370.
33 M. Liu, J. L. Kan, Y. Q. Yao, Y. Q. Zhang, B. Bian, Z. Tao, Q. J. Zhu and X. Xiao, Facile preparation and application of luminescent cucurbit[10]uril-based porous supramolecular frameworks, *Sens. Actuators, B*, 2019, **283**, 290–297.
34 J. Murray, K. Kim, T. Ogoshi, W. Yao and B. C. Gibb, The aqueous supramolecular chemistry of cucurbit[*n*]urils, pillar[*n*]arenes and deep-cavity cavitands, *Chem. Soc. Rev.*, 2017, **46**, 2479–2496.
35 W. Liu, S. K. Samanta, B. D. Smith and L. Isaacs, Synthetic mimics of biotin/(strept) avidin., *Chem. Soc. Rev.*, 2017, **46**, 2391–2403.
36 X. L. Ni, S. X. Cao, P. Wang, X. Zeng and Z. Tao, Cucurbiturils-catalyzed tunable carbon dots from single organic precursors in water, *Org. Chem. Front.*, 2021, **8**, 224–230.
37 S. Zhang, Y. Tian, M. Liu, T. H. Meng, C. R. Li, X. Zeng, X. Xiao and C. Redshaw, A cucurbit[6]uril-carbon dot system: a potentially new bioimaging agent, *Mater. Chem. Front.*, 2022, **6**, 973–980.
38 Z. Qian, J. Ma, X. Shan, H. Feng, L. Shao and J. Chen, Highly luminescent N-doped carbon quantum dots as an effective multifunctional fluorescence sensing platform, *Chemistry*, 2014, **20**, 2254–2263.
39 X. Shan, L. Chai, J. Ma, Z. Qian, J. Chen and H. Feng, B-doped carbon quantum dots as a sensitive fluorescence probe for hydrogen peroxide and glucose detection, *Analyst*, 2014, **139**, 2322–2325.
40 A. B. Bourlinos, G. Trivizas, M. A. Karakassides, M. Baikousi, A. Kouloumpis, D. Gournis, A. Bakandritsos, K. Hola, O. Kozak, R. Zboril, I. Papagiannouli, P. Aloukos and S. Couris, Green and simple route toward boron doped carbon dots with significantly enhanced non-linear optical properties, *Carbon*, 2015, **83**, 173–179.
41 Y. Han, D. Tang, Y. Yang, C. Li, W. Kong, H. Huang, Y. Liu and Z. Kang, Non-metal single/dual doped carbon quantum dots: a general flame synthetic method and electro-catalytic properties, *Nanoscale*, 2015, **7**, 5955–5962.
42 Q. Xu, P. Pu, J. Zhao, C. Dong, C. Gao, Y. Chen, J. Chen, Y. Liu and H. Zhou, Preparation of highly photoluminescent sulfur-doped carbon dots for Fe(iii) detection, *J. Mater. Chem. A*, 2015, **3**, 542–546.
43 S. Yang, J. Sun, P. He, X. Deng, Z. Wang, C. Hu, G. Ding and X. Xie, Selenium Doped Graphene Quantum Dots as an Ultrasensitive Redox Fluorescent Switch, *Chem. Mater.*, 2015, **27**, 2004–2011.
44 T. Y. Luo, X. He, J. Zhang, P. Chen, Y. H. Liu, H. J. Wang and X. Q. Yu, Photoluminescent F-doped carbon dots prepared by ring-opening reaction for gene delivery and cell imaging, *RSC Adv.*, 2018, **8**, 6053–6062.
45 Y. Z. Zhang, M. Q. Xu, X. K. Liu, M. Wang, J. Zhao, S. Li and M. Yin, Regulation of biochar mediated catalytic degradation of quinolone antibiotics: Important role of environmentally persistent free radicals, *Bioresour. Technol.*, 2021, **326**, 124780.
46 A. Day, A. P. Arnold, R. J. Blanch and B. Snushall, Controlling Factors in the Synthesis of Cucurbituril and Its Homologues, *J. Org. Chem.*, 2001, **66**, 8094–8100.
47 H. Ming, Y. Yan, J. Ming, X. Li, Q. Zhou, H. Huang and J. Zheng, Porous TiO_2 nanoribbons and TiO_2 nanoribbon/

carbon dot composites for enhanced Li-ion storage, *RSC Adv.*, 2014, **4**, 12971–12976.

48 T. Yuan, F. L. Yuan, X. H. Li, Y. C. Li, L. Z. Fan and S. H. Yang, Fluorescence-phosphorescence dual emissive carbon nitride quantum dots show 25% white emission efficiency enabling single-component WLEDs, *Chem. Sci.*, 2019, **10**, 9801–9806.

49 J. Y. Zhu, X. Bai, X. Chen, H. Shao, Y. Zhai, G. C. Pan, H. Z. Zhang, E. V. Ushakova, Y. Zhang, H. W. Song and A. L. Rogach, Spectrally Tunable Solid State Fluorescence and Room-Temperature Phosphorescence of Carbon Dots Synthesized *via* Seeded Growth Method, *Adv. Opt. Mater.*, 2019, **7**, 1801599.

50 D. Qu and Z. C. Sun, The formation mechanism and fluorophores of carbon dots synthesized *via* a bottom-up route, *Mater. Chem. Front.*, 2020, **4**, 400–420.

51 M. Y. Liang, Z. C. Liu, Z. H. Zhang, Y. X. Mei and Y. Tian, A two-photon ratiometric fluorescent probe for real-time imaging and quantification of NO in neural stem cells during activation regulation, *Chem. Sci.*, 2022, **13**, 4303–4312.

52 H. L. Zhang, Y. F. Gao, Y. Jiao, W. J. Lu, S. M. Shuang and C. Dong, Highly sensitive fluorescent carbon dots probe with ratiometric emission for the determination of ClO^-, *Analyst*, 2020, **145**, 2212.

53 Z. Yang, T. T. Xu, X. Zhang, H. Li, X. D. Jia, S. S. Zhao, Z. W. Yang and X. R. Liu, Nitrogen-doped carbon quantum dots as fluorescent nanosensor for selective determination and cellular imaging of ClO^-, *Spectrochim. Acta, Part A*, 2022, **271**, 120941.

54 D. Hong, X. Y. Deng, J. M. Liang, J. Y. Li, Y. Tao and K. J. Tan, One-step hydrothermal synthesis of down/up-conversion luminescence F-doped carbon quantum dots for label-free detection of Fe^{3+}, *Microchem. J.*, 2019, **151**, 104217.

55 C. Kang, S. Tao, F. Yang and B. Yang, Aggregation and luminescence in carbonized polymer dots, *Aggregate*, 2022, **3**, e169.